ACS MEASUREMENT SCIENCE Au
AN OPEN ACCESS JOURNAL OF THE AMERICAN CHEMICAL SOCIETY

pubs.acs.org/measureau
Article

MXene Nanosheets-Decorated Paper as a Green Electronics Material for Biosensing

Shan-Chu Yu, Tzu-Yen Huang, and Tzu-En Lin*

Cite This: ACS Meas. Sci. Au 2024, 4, 81−91
Read Online

ACCESS | Metrics & More | Article Recommendations | Supporting Information

ABSTRACT: This research delves into the development and optimization of MXene nanosheet-based paper electrodes, emphasizing their adaptability in green electronics and diverse applications. Xuan paper, a cellulose-based material, was identified as an ideal substrate for its mechanical attributes and capacity to accommodate MXene, further yielding outstanding electrical conductivity. The MXene paper electrode demonstrated consistent performance under various conditions, showing its potential in the field of wearable electronics and medical devices. Notably, its impressive electrothermal capabilities and environmentally conscious decomposition mechanism make it a promising candidate for future green electronic applications. Overall, this study underscores the electrode's harmonization of performance and environmental sustainability, paving the way for its integration into futuristic electronic solutions.

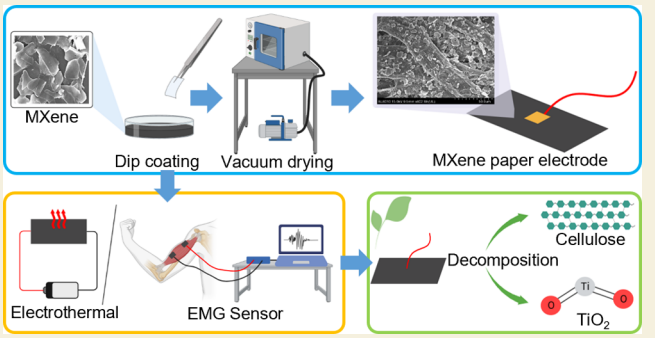

KEYWORDS: *MXene nanosheets, paper electrode, green electronics, Xuan paper, wearable devices, electrothermal performance, sustainable design*

1. INTRODUCTION

Consumers' growing interest in purchasing new electronic products plays a pivotal role in the rapid expansion of the world's fastest-increasing waste stream—electronic waste. This escalating issue has become an environmental hazard due to its toxic legacy.[1,2] In recent times, an increasing spotlight has been cast on the emergence of green electronics.[3−5] The emerging field of green electronics is focused on designing and manufacturing electronic devices that have a minimal impact on the environment. Across the globe, researchers and scientists are actively investigating diverse strategies to attain sustainable and eco-conscious solutions within the realm of electronic device manufacturing.

Numerous noteworthy studies have advanced this research domain by introducing innovative materials derived from lignocellulose, chitin, fibrin, and other biomass sources.[6−11] For example, Silvestre et al. conducted a study on cork-derived laser-induced graphene for sustainable green electronics. Their eco-friendly approach involved a single-step direct laser writing method to produce flexible electrodes.[12] Fu et al. conducted pioneering research on flexible electronics based on wood. Additionally, a sustainable and bioderived conductive ink was developed, incorporating carbon nanofibers derived from lignin.[13] These studies, along with other recent influential works such as those by Xu et al., Lovley et al., Monroe et al., Min et al., and Tong et al., collectively contribute to the growing body of knowledge in green electronics.[14−18]

The paper stands out as the most affordable and widely used flexible substrate in everyday life. Its production involves dehydrating a diluted mixture of cellulose fibers, a process followed by filtration, pressing, and heating. The fiber-laden water suspension, known as pulp, is primarily derived from wood through mechanical, thermomechanical, or chemical means that separate its constituent fibers. The characteristics of paper substrates can exhibit significant variations, contingent upon their composition and structure. While some papers offer opacity, others provide translucence; absorbency can differ significantly, with some rapidly imbibing liquids and others showing resistance. The particular demands for these attributes hinge upon the intended application of the paper substrate.

Although consideration of the electrical characteristics of paper becomes especially pertinent when integrating electronics onto paper substrates, it is noteworthy that paper stands as an environmentally friendly and recyclable material, making it a promising candidate for electronics fabrication.[19,20] Yet, by its nature, paper inherently functions as an insulator. Overcoming this challenge to render paper more conductive is

Received: August 25, 2023
Revised: October 17, 2023
Accepted: October 23, 2023
Published: November 9, 2023

Scheme 1. (a) Schematic Illustration Depicting the Fabrication Process of the MXene Paper Electrode; (b) The Wearable Sensor Electrode Serves a Dual Purpose: It Can Be Applied for Electrothermal Therapy or Function as an Emg Sensor; (c) Over Time, the Electrode Can Naturally Degrade into Cellulose Fragments and TiO_2 Components

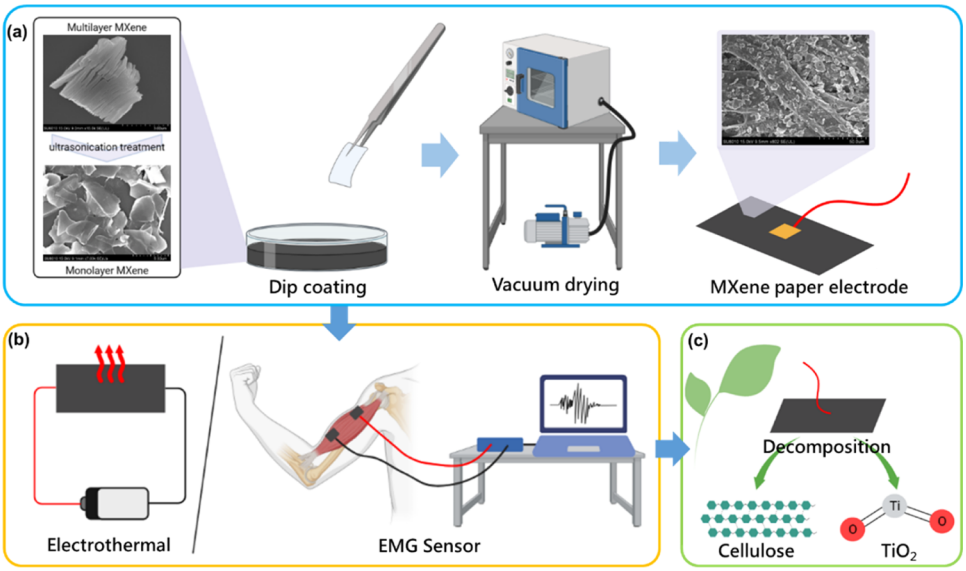

of paramount importance. Typically, scientists resort to the application of conductive ink for this purpose. However, conventional inks often lack biocompatibility and degradability. In this study, we leverage MXene nanosheets, a 2D material, to serve as conductive ink for enhancing the paper's conductivity.

In this study, we aim to explore the potential of combining the remarkable properties of MXene ($Ti_3C_2T_x$), an emerging 2D material known for its outstanding conductivity, biocompatibility, and cost-effectiveness, with metal nanoparticles.[21−23] Many papers have highlighted the utility of metal nanoparticles on 2D materials, making it essential to investigate the performance of gold nanoparticle-decorated MXene (Au@MXene) and pristine MXene nanosheets-decorated paper electronics.[24−26] MXene's surface features terminal functional groups such as hydroxyl (−OH), oxygen (−O), and fluorine (−F), endowing it with hydrophilicity and enabling solution-based processing.[27] In particular, these functional groups or nanoparticles give them the ability to respond rapidly and stably to low voltages by Joule heating, suggesting potential applications in electrothermal therapy.[23,28] Beyond simply enhancing the performance of traditional electronic devices, the MXene-decorated paper in this work promises to open up entirely new avenues of applications. The exceptional breathability of paper makes it an ideal choice for designing soft biomedical sensors, particularly those intended for direct skin contact. Therefore, within this study, we fused the highly conductive MXene nanosheets or Au@MXene with the flexibility and breathability of paper, resulting in the creation of groundbreaking epidermal electrodes.

2. MATERIALS AND METHODS

2.1. Materials and Chemicals

MXene ($Ti_3C_2T_x$) was purchased from XinXi-technology. Chloroauric acid ($HAuCl_4{\cdot}4H_2O$, 99.99%) was bought from ACROS. Ethanol (C_2H_5OH, 99.5%) was purchased from Echo Chemical. Sodium hydroxide (NaOH) was purchased from ACROS. Xuan paper was purchased from ChungHua Pencil Company that is composed of approximately 40% Wikstroemia sikokiana fiber and 60% rice straw fibers. Conventional Ag/AgCl electrodes were purchased from Kendall Meditrace. Ultrapure deionized water was obtained from Sartorius (18.25 MΩ·cm, 25 °C) and was used in all experiments.

2.2. Preparation of Monolayer MXene Nanosheets

A 100 mg portion of multilayer MXene nanosheets was dispersed in 5 mL of ultrapure water, followed by ultrasonication treatment at 100 W for 2 h. Subsequently, we introduced 15 mL of anhydrous ethanol into the MXene nanosheets solution.

2.3. Preparation of Au@MXene Nanosheets

100 mg amount of multilayer MXene nanosheets was dispersed in 5 mL of ultrapure water, followed by ultrasonication treatment at 100 W for 2 h. Subsequently, we added 15 mL of ultrapure water and introduced 100 mM tetrachloroauric acid, allowing the reaction to proceed for 10 min. Afterward, the resulting product underwent centrifugation at 4400 rpm for 20 min. Finally, we redispersed Au@MXene nanosheets in 20 mL of ethanol for further utilization.

2.4. Preparation of MXene Nanosheet-Based Paper Electrode and Au@MXene Nanosheets-Based Paper Electrode

In this experiment, we used a fast, simple, and inexpensive dip-coating technique to fabricate MXene nanosheet-based paper electrodes. The paper was first cut to a standard size of 15 mm in width and 30 mm in length. The paper strips were then dipped into the previously prepared MXene nanosheets suspension or Au@MXene nanosheets suspension for 30 s and then vacuum-dried in a 40 °C vacuum oven for 15 min. To further improve the conductivity, we repeated the dipping and drying procedures several times until the conductivity reached the desired level.

2.5. Characterization of MXene Nanosheets

The surface morphology and microstructure of the samples were examined using scanning electron microscopy (SEM, Hitachi SU-8010, Japan) under an acceleration voltage of 15 kV. The elemental composition of the samples was analyzed by energy-dispersive X-ray spectroscopy (EDS, Hitachi SU-8010, Japan). The geometrical features of the samples were observed by using a transmission electron microscope (TEM, Hitachi HT7800, Japan). The crystalline structures of the samples were analyzed by X-ray diffraction (XRD, PANalytical Empyrean, U.K.). A qualitative analysis of the samples was performed by UV−visible spectroscopy (CLARIOstar BMG LABTECH, Germany). Sample temperature and infrared images were

https://doi.org/10.1021/acsmeasuresciau.3c00043
ACS Meas. Sci. Au 2024, 4, 81−91

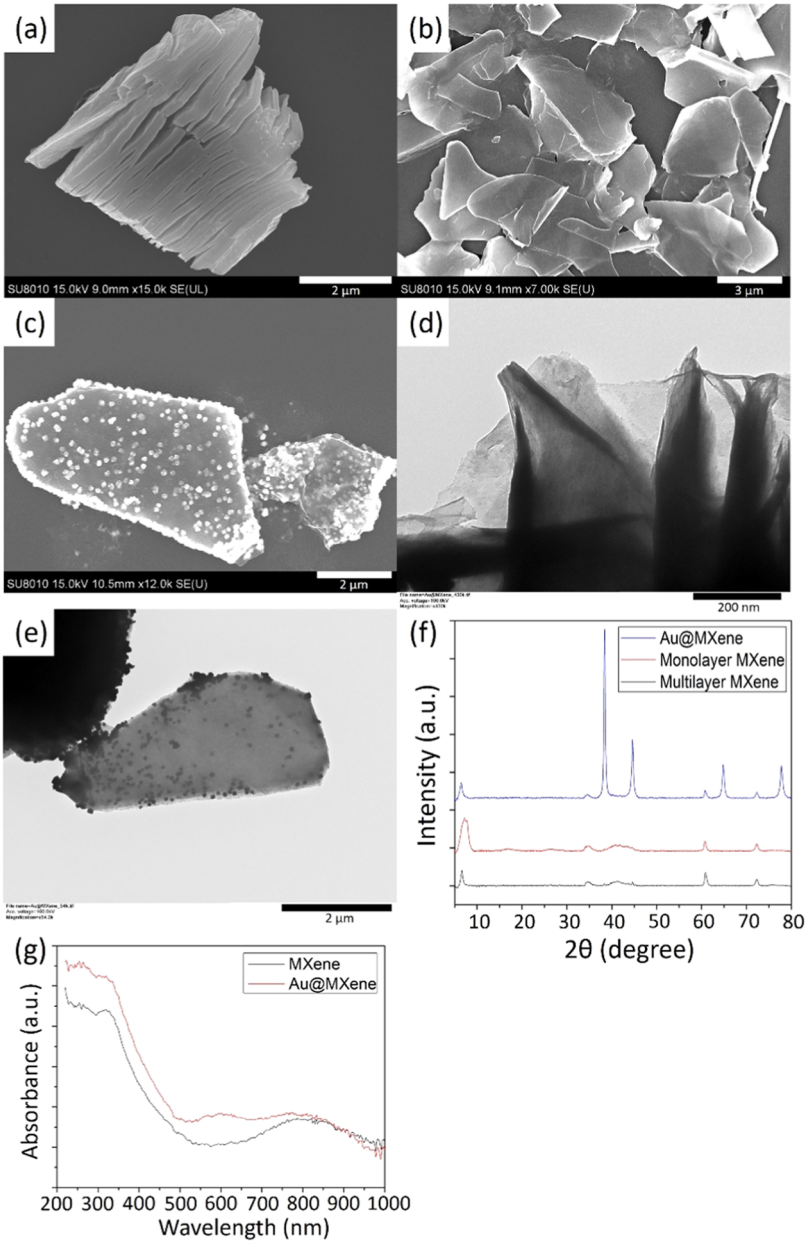

Figure 1. (a–c) SEM images of (a) multilayer MXene, (b) monolayer MXene, and (c) Au@MXene. (d, e) TEM images of (d) monolayer MXene and (e) Au@MXene. (f) XRD pattern of multilayer MXene (black line), monolayer MXene (red line), and Au@MXene (blue line). (g) UV–visible spectra of MXene and Au@MXene colloidal solutions.

recorded by using an infrared thermography camera (FLIR E5 XT). The volumetric conductivity of the samples ($\sigma = L/RS$, where S and L represent the cross-sectional area and the distance between the electrodes, respectively) was derived from the volumetric resistance (R) measured with an electrometer (Keithley 6514). The electrothermal power was applied via a direct current source from a power supply (GWinstek GPD-4303S, Taiwan). The prepared sensor was attached to the human body by using transparent breathable medical tape to detect electromyography (EMG) signals during human movement. The surface electromyography (EMG) recording system comprises an STM32 microcontroller (STMicroelectronics NUCLEO-L031 K6, France) and a Muscle Sensor (MyoWare AT-04-001). The STM32 microcontroller is directly interfaced with the Muscle Sensor and transmits data to the computer via a wired connection.

3. RESULTS AND DISCUSSION

3.1. Design of the MXene Nanosheet-Based Paper Electrodes

The selection of an appropriate substrate is pivotal in the construction of green electronics, providing essential mechanical support and ensuring physical stability. Among the various options available, cellulose-based materials, including commonly observed papers, emerge as optimal candidates due to their inherent flexibility. The comprehensive versatility of MXene nanosheet-based paper electrodes is illustrated in Scheme 1. In Scheme 1(a), the schematic representation elucidates the intricate fabrication process, providing insights into the creation of this innovative electrode. Scheme 1(b) underscores the electrode's multifunctionality by accentuating its dual capacity as a potential component for both

https://doi.org/10.1021/acsmeasuresciau.3c00043
ACS Meas. Sci. Au 2024, 4, 81–91

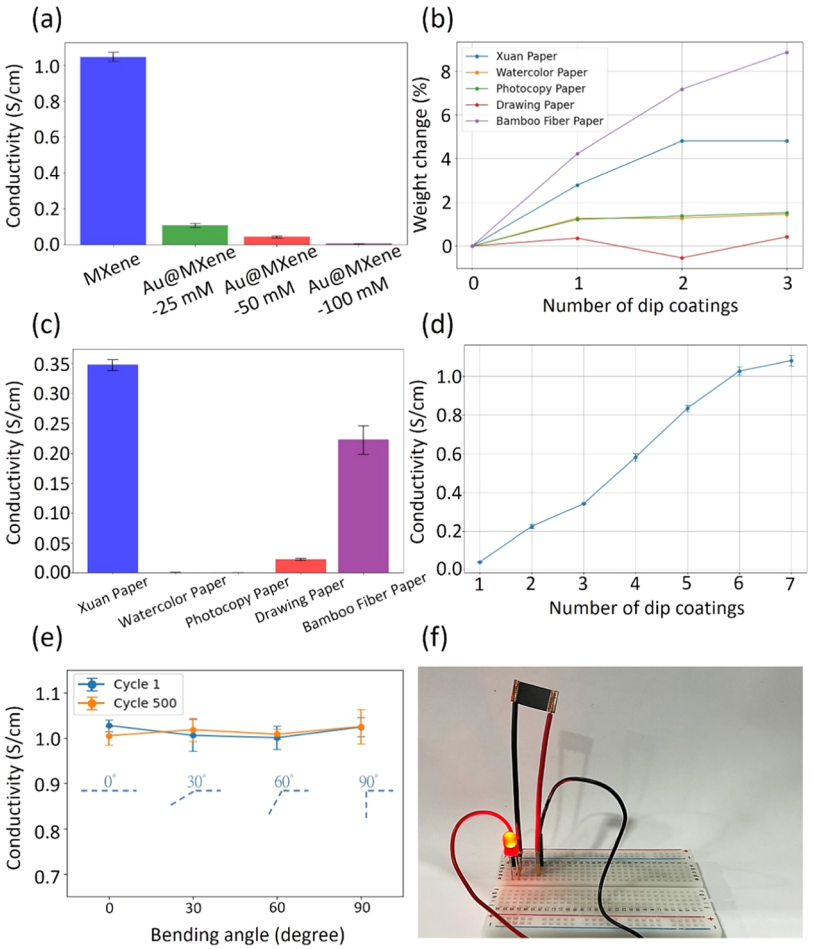

Figure 2. (a) Conductivity of the MXene paper electrode and Au@MXene paper electrode. (b) Percentage change in weight of different types of paper coated with MXene solution three times. (c) Conductivity of different types of paper coated with MXene solution after three dip-coating cycles. (d) Conductivity of the MXene paper electrode as a function of dip-coating times. (e) Relationship between bending angle and conductivity. (f) MXene paper electrode is used as part of the wire leads in circuits. Each experiment was conducted in three independent replicates ($N = 3$) to ensure the reliability of the results.

electrothermal therapy and EMG sensing applications, showcasing its adaptability across diverse domains of medical and technological progress. Furthermore, Scheme 1(c) introduces an intriguing facet of sustainability and eco-friendliness. This electrode showcases a distinct ability to undergo decomposition into cellulose fragments and TiO_2 elements, aligning with contemporary endeavors to engineer materials that not only excel in performance but also embrace a circular and environmentally conscious design philosophy.[29,30]

3.2. Characterization of MXene nanosheets

In this study, two types of MXene nanosheets were examined: monolayer $Ti_3C_2T_x$ MXenes and monolayer Au nanoparticle-decorated $Ti_3C_2T_x$ MXenes, referred to as Au@MXene. The surface characteristics of both MXene and Au@MXene were assessed by using SEM and TEM techniques. Analysis of Figure 1(b),(d), clearly reveals the monolayer sheet-like structure of the synthesized MXene, aligning well with the defining traits of 2D nanomaterials, MXenes. Notably, our MXene synthesis process prevents the formation of a multilayer accordion-like configuration due to the implementation of an ultrasonication treatment. This treatment effectively disperses the MXene into single-layer structures within the solution. In contrast to the multilayer MXene illustrated in Figure 1(a), the monolayer MXene displays a significantly augmented specific surface area and more uniform dispersion in the solution. This advantageous feature enhances the conductivity network upon application onto paper fibers, resulting in notable advancements in the electrode performance.

To conduct a thorough comparison with MXene and MXene decorated with nanoparticles, we synthesized hybrid composites by introducing gold nanoparticles into MXene. These composites were denoted as Au@MXene, resulting in 0D+2D nanocomposites. As depicted in Figure 1(c),(e), a uniform distribution of gold nanoparticles embellishes the two-dimensional sheet-like MXene structure, with nanoparticle diameters typically falling within the range of 70 to 80 nm.

X-ray diffraction (XRD) analysis was performed to verify the crystalline structures of multilayer MXene, monolayer MXene, and Au@MXene, the results of which are shown in Figure 1(f). The multilayer MXene showed main diffraction peaks of MXene ($Ti_3C_2T_x$) at 6.7 and 60.9°, which correlate with the (002) and (110) crystal planes, as referenced in ref 31. The red line indicates the monolayer of MXene after ultrasound treatment. Its diffraction peak positions were analogous to the multilayer MXene, but with a more pronounced (002) crystal plane diffraction peak, possibly due to increased surface area or reduced interlayer interactions in the monolayer

https://doi.org/10.1021/acsmeasuresciau.3c00043
ACS Meas. Sci. Au 2024, 4, 81−91

MXene. For Au@MXene, represented by the blue line, the integration of AuNPs did not obscure the original MXene peaks. Additional peaks aligned with the (111) and (200) planes of Au were observed, confirming the face-centered cubic crystal structure of Au and the successful preparation of Au@MXene.

An in-depth study of the optical properties of MXene and Au@MXene was then characterized by using a UV−visible spectrophotometer, as shown in Figure 1(g). Distinct MXene absorption peaks at 325 and 770 nm were detected in both sample types, consistent with previous studies.[32] Notably, an additional absorption peak at around 580 nm was identified exclusively in the Au@MXene samples, corresponding to gold nanoparticles, confirming the successful formulation of the Au@MXene composite (Satheeshkumar et al.).[33]

3.3. Paper-Type Selection

Both MXene nanosheets and Au@MXene nanosheets underwent dip coating for testing purposes. It became evident that the performance of the MXene nanosheets, in terms of conductivity and stability, surpassed that of the Au@MXene nanosheets. As a result, MXene nanosheets were selected for subsequent experiments. The findings illustrated in Figure 2(a) yielded a surprising outcome. For clarity, in this study, different concentrations of gold added were denoted as Au@MXene-25 mM, Au@MXene-50 mM, and Au@MXene-100 mM. The concentration in these abbreviations represents the concentration of tetrachloroauric acid used during the preparation of Au@MXene, indicating the content of gold in the respective samples. Following six applications of either 5 mg/mL MXene or Au@MXene, paper electrodes crafted with Au@MXene exhibited a notable decline in conductivity. Moreover, this reduction was more pronounced with a higher content of gold nanoparticles. Plausible insight into these results arises from the mismatch between the face-centered cubic lattice structure of gold crystals and the hexagonal arrangement found in MXene, which encompasses variations in the atomic dimensions. This disparity between gold nanoparticles and MXene within Au@MXene could give rise to lattice distortions or other irregularities that hinder the movement of charge carriers, leading to an increase in resistance. Additionally, the self-reduction process involving gold ions utilized in the creation of Au@MXene might lead to the oxidation of certain Ti atoms on the MXene surface. This chemical reaction could disrupt the MXene structure and subsequently elevate resistance. Both of these hypotheses credibly account for the observed decrease in conductivity, particularly with an increase in the gold nanoparticle concentration. Consequently, Au@MXene is not appropriate for use as a sensing nanomaterial in this case. Ultimately, pure MXene (devoid of Au) was selected as the sensing nanomaterial for the fabrication of green electronics.

As depicted in Figure 2(b),(c), various paper types, including Xuan paper, watercolor paper, drawing paper, photocopy paper, and bamboo fiber paper, were immersed in the pure MXene solution, inducing alterations in both their weight and their electrical conductivity. Notably, an incremental weight gain across all paper variants became evident with each successive immersion, following a linear trend. This trend could be attributed to the gradual infiltration of MXene into the paper's pores during each immersion, leading to the accumulation of MXene within the paper. Noteworthy was the observation that Xuan paper displayed a distinct rise in weight after the first and second immersions, albeit with diminishing prominence after the third dip-coating cycle. This phenomenon could be attributed to the saturation of Xuan paper's surface fibers by MXene, resulting in effective coverage.

In Figure 2(c), the electrical conductivity of all paper types was compared after the paper underwent three dip-coating cycles. Xuan paper, after being subjected to three MXene dip-coating treatments, distinctly distinguished itself, boasting the highest electrical conductivity of 0.3467 S/cm. This exceptional conductivity could be attributed to the inherent MXene absorption capacity of Xuan paper fibers, coupled with their structural propensity to foster the establishment of conductive networks. Consequently, Xuan paper surpassed bamboo fiber paper, which demonstrated a higher rate of weight alteration. This elevated conductivity underscored the successful development of a well-structured conductive network on the surface of Xuan paper fibers, facilitating efficient electrical conduction. Consequently, this augmented the efficacy of EMG signal capture.

Based on the amalgamation of the aforementioned experimental findings, it was deduced that Xuan paper emerged as the optimal choice for the fabrication of MXene paper electrodes. Its exceptional MXene carrier capacity substantiated its suitability in this application.

3.4. Optimization of MXene Paper Electrodes

To increase the conductivity of the MXene paper electrodes, we adopted a method of increasing the number of dip-coatings. Figure 2(d) clearly shows the relationship between the number of dip-coatings and the conductivity. The data show that with only one MXene dip-coating, the conductivity is as low as 0.0405 S/cm. This result suggests that the MXene layer is still thin, and the conductive network is not fully formed, limiting the conductivity. However, when the number of dip-coatings reaches three, the conductivity increases to 0.3405 S/cm, showing a clear improvement. As we continue to increase the number of dip-coatings, the conductivity continues to increase, peaking at 1.0428 S/cm after the seventh dip-coating. This result suggests that at this stage, the MXene conductive network has reached a sufficient thickness on the surface of the paper fibers to effectively improve the overall conductivity. Notably, there is a significant slowdown in the rate of conductivity growth as the number of dip-coatings continues to increase between six and seven. This could indicate that the MXene layer has reached an optimum thickness, and further dip-coatings may not significantly increase the conductivity. Keeping in mind the balance between the manufacturing cost and material performance, we decided to perform six dip-coatings in the MXene paper electrode fabrication experiment.

3.5. Bending Stability Tests and the Application in Circuit

As shown in Figure 2(e), this study demonstrated the conductivity stability of the MXene paper electrode under different bending angles. The results indicated that the conductivity of the MXene paper electrode remained stable during bending, with no significant impact within a bending range of 0 to 90°, and maintained almost constant conductivity even after 500 bending cycles. This observation was of paramount importance for applications involving skin patch electrodes. Given that the skin presents a dynamic surface, the electrodes could undergo diverse bends and strains as the user moves. Consequently, maintaining stable conductivity under bending conditions was vital to ensure a consistent signal

https://doi.org/10.1021/acsmeasuresciau.3c00043
ACS Meas. Sci. Au 2024, 4, 81−91

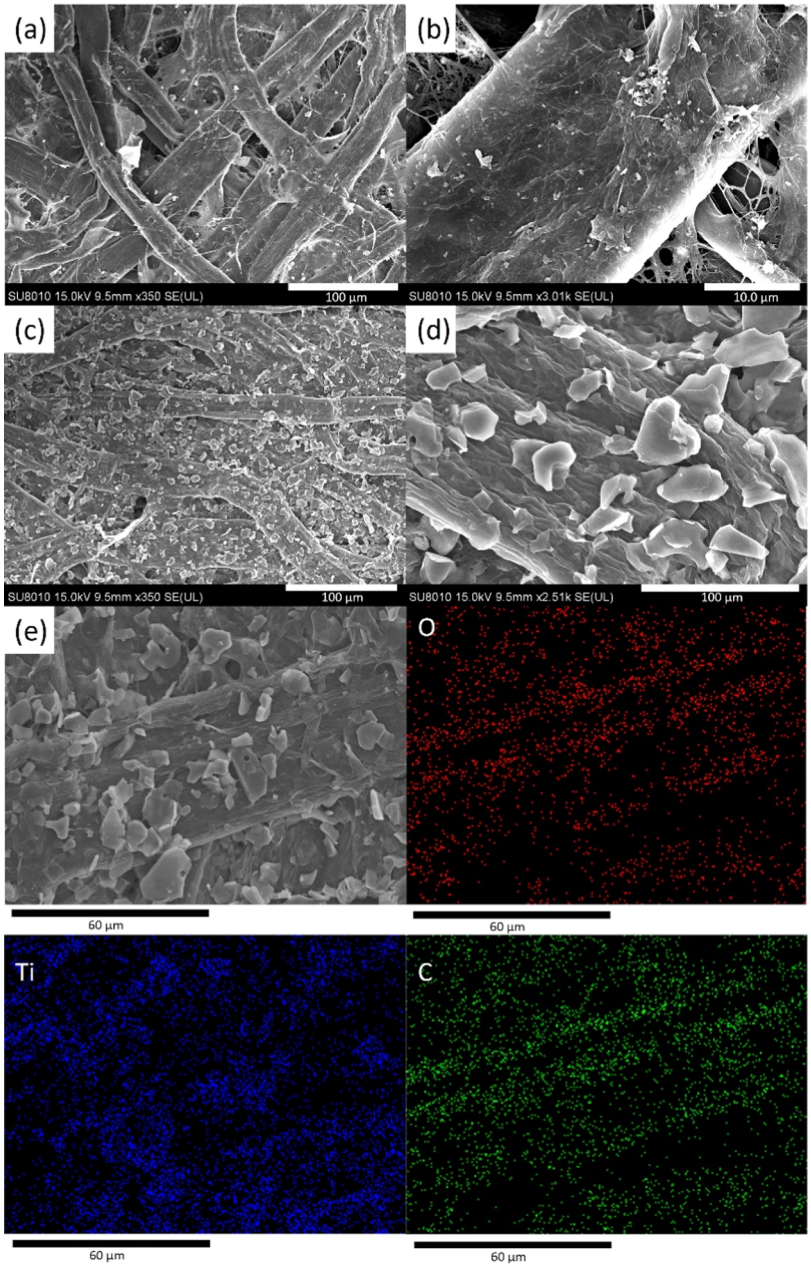

Figure 3. SEM images of the Xuan paper surface at (a) low magnification and (b) high magnification. (c, d) SEM images of the MXene paper electrode surface at (c) low magnification and (d) high magnification. (e) EDS element mapping of the surface of the MXene paper electrode.

output in dynamic scenarios. The showcased high mechanical flexibility and conductivity stability of the MXene paper electrode position it as an ideal choice for applications necessitating heightened adaptability and reliability, such as wearable medical devices or sports monitoring systems. Moreover, it underscored the potential applicability of MXene paper electrodes in forthcoming electronic skin and other flexible electronic devices.

Furthermore, we successfully used MXene Paper as a conductor in a circuit, effectively illuminating an LED as shown in Figure 2(f). This result underscores not only the exceptional conductive properties of MXene Paper but also its viability as an effective alternative material in real-world electronic applications.

3.6. Characterization of MXenes Nanosheets on Xuan Paper

As shown in Figure 3(a),(b), the SEM images depict the surface morphology of the Xuan paper. At lower magnification, the overall fiber network structure of the Xuan paper is evident, while at higher magnification, the microstructural details of the fibers are clearly visible. These images provide us with the basic structural characteristics of the original Xuan paper. Figure 3(c),(d) shows the surface of the paper fiber electrode after MXene modification. The low-magnification SEM images show the uniform distribution of MXene nanosheet over the fibers. The high-magnification images, on the other hand, clearly show features consistent with the monolayer MXene morphology previously captured by SEM. The uniform MXene coating on the paper fiber electrode likely imparts a significant conductivity enhancement to the paper. In addition, the EDS

https://doi.org/10.1021/acsmeasuresciau.3c00043
ACS Meas. Sci. Au 2024, 4, 81−91

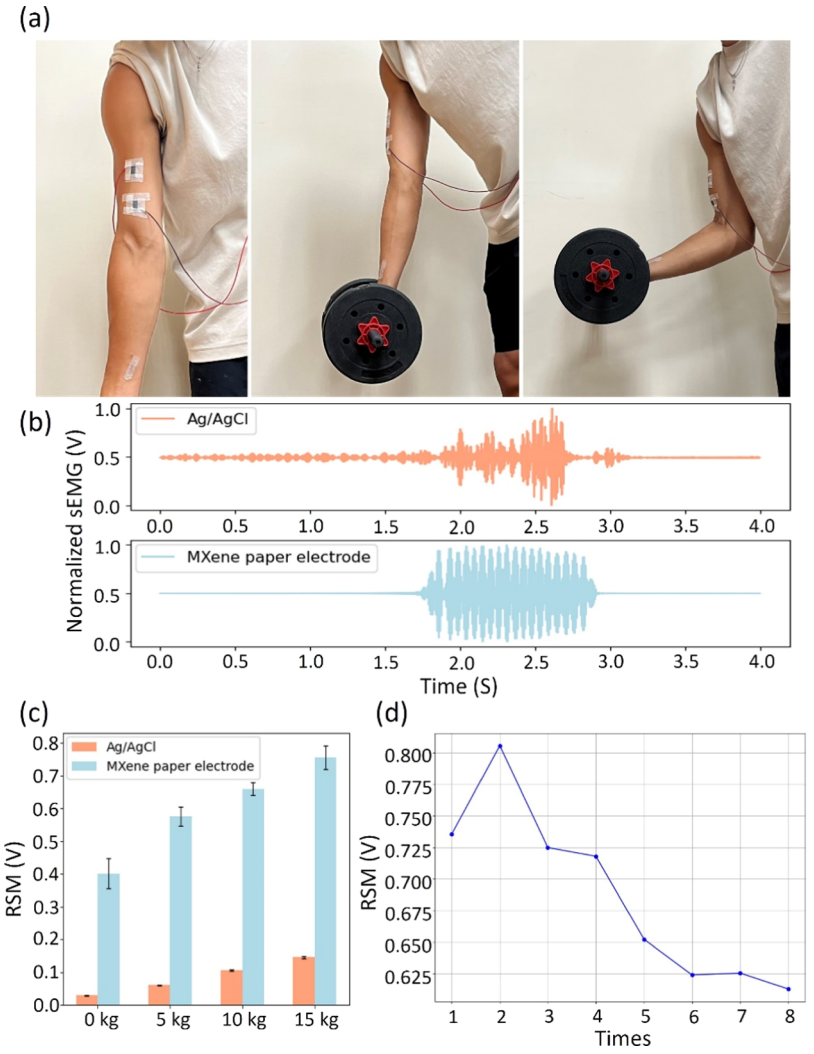

Figure 4. (a) Schematic representation illustrating the placement of electrodes and the measurement of biceps brachii electromyography (EMG) signals. (b) EMG waveform graphs of Ag/AgCl and MXene paper electrodes. (c) Electromyography (EMG) signals recorded from the biceps brachii muscle during the exertion of lifting dumbbells of four distinct weights (N = 3). (d) Variations in the electromyography (EMG) signals captured from the biceps brachii muscle when exerting force to lift a 15 kg dumbbell for a total of eight repetitions.

elemental mapping results in Figure 3(e) reveal the elemental distribution on the MXene paper electrode surface. The mappings show the presence of Ti, O, and C on the MXene paper. The homogeneous distribution of Ti confirms the successful modification with MXene ($Ti_3C_2T_x$), while the distribution of the C and the O elements delineates the original paper fiber structure. Since the content of MXene is not the main constituent, the observed signals of C and O elements are largely attributed to cellulose. Combining the above results, it can be concluded that this study successfully achieved a uniform MXene coating on the surface of Xuan paper, and the EDS results further confirm this successful modification. In addition, the MXene-modified Xuan paper may exhibit improved electrical conductivity, a hypothesis to be further explored in subsequent experiments.

3.7. Application and Performance of MXene Paper Electrodes in EMG Signal Measurement

We used MXene paper electrodes to measure the EMG signals of the biceps brachii (as illustrated in Figure 4(a)) and compared the acquired EMG signals during the lifting of dumbbells weighing 0, 5, 10, and 15 kg. The waveform of the EMG signals, shown in Figure 4(b), was compared to that of commercially available Ag/AgCl electrodes. It was observed that the MXene paper electrode had a relatively stable baseline compared to the commercial electrodes, indicating that the MXene paper electrode can achieve a lower noise level when measuring EMG signals. The system for measuring EMG is shown in Figure S1 and includes the STM32 NUCLEO-L031 K6 microcontroller and the MyoWare muscle sensor. The STM32 microcontroller interfaces with the MyoWare muscle sensor to convert analog signals to digital format and then transmits the data to a computer. The technique for connecting the MXene paper electrode to copper wires is shown in Figure S2, where copper tape is used to adhere the wire to the MXene paper electrode. After acquiring the EMG signals, we calculated the root-mean-square (RMS) values using the following formula

$$\mathrm{RMS} = \sqrt{\frac{1}{N}\sum_{i=1}^{N} x_i^2}$$

where x_i represents each sample value of the EMG signal and N represents the number of samples. Figure 4(c) shows that as

https://doi.org/10.1021/acsmeasuresciau.3c00043
ACS Meas. Sci. Au 2024, 4, 81−91

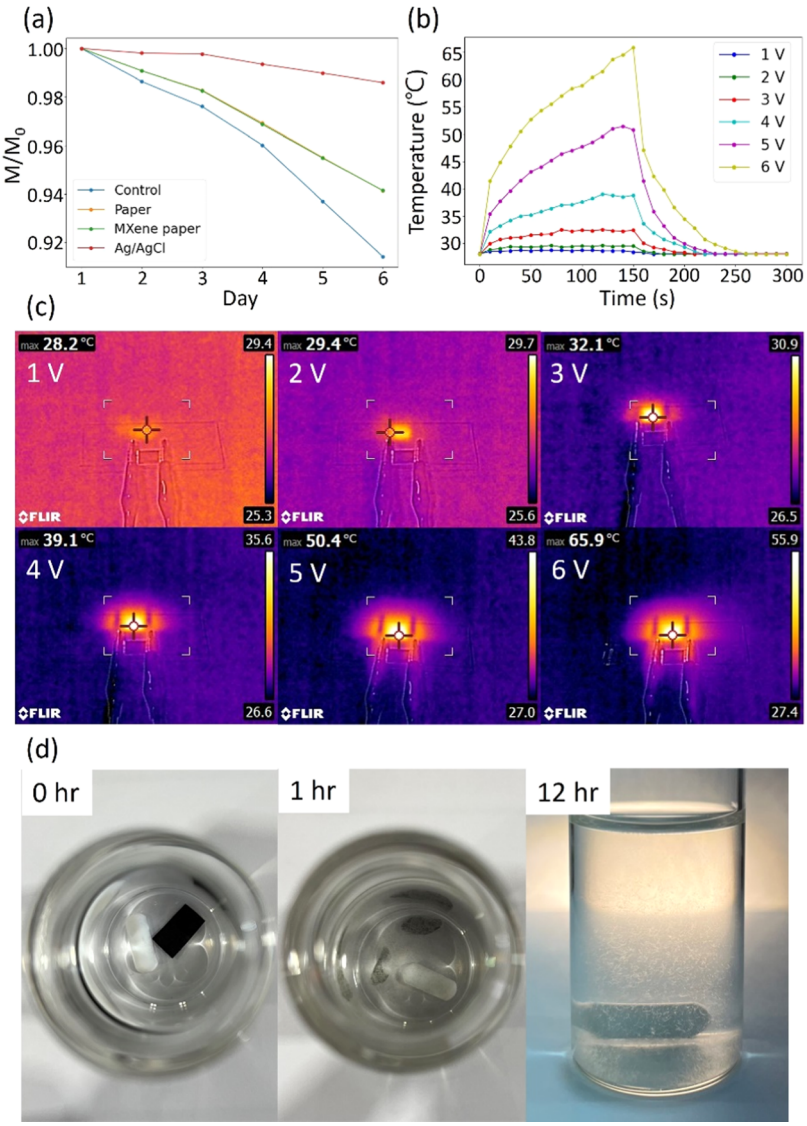

Figure 5. (a) Air permeability tests. M_0 represents the original weight, while M means the weight measured. (b) Electrothermal performances of MXene paper electrode at input voltages of 1, 2, 3, 4, 5, and 6 V. (c) Infrared thermal images capturing the peak temperature variations of MXene paper electrodes subjected to different applied voltage levels. (d) Analysis of the decomposition behavior of MXene paper electrodes when immersed in a 5 M NaOH solution.

the weight of the dumbbell increased, the RMS value derived from the measured EMG signal also increased accordingly. This observation is consistent with the established relationship between muscle activity and load carried. As muscles are required to generate greater force to lift heavier objects, the activity of the muscle fibers increases, resulting in an amplified EMG signal. We also compared the sensitivity of the commercially available Ag/AgCl electrode and the MXene paper electrode. It is observed that the RMS peak of the MXene paper electrode is superior to the commercial Ag/AgCl electrode under all weights, and the magnitude of the increase is significantly more pronounced. This result further substantiates that our MXene paper electrode has exemplary sensitivity and also indicates that the MXene paper electrode can more accurately detect muscle changes and provide more reliable signals. A key advantage of the MXene paper electrode is its exceptional sensitivity, simplicity, and portability. This provides a notable advantage in real-time monitoring and analysis of EMG signals, especially in scenarios where speed, accuracy, and convenience are required.

Figure 4(d) shows the variation in the RMS values of the EMG signals as the biceps brachii were subjected to lifting a 15 kg dumbbell, the maximum weight the participant could lift. Preliminary data indicate that the RMS value at the beginning of the lift was 0.735 V, which increased to 0.806 V during the second attempt. Surprisingly, however, as the number of lifting repetitions increased, the RMS value showed a gradual decline, dropping to 0.613 V by the eighth repetition. It is generally accepted that as muscles fatigue, the body recruits more muscle fibers to perform the same movement, resulting in an increase in the RMS value of the EMG. However, our observations seem to contradict this notion. This discrepancy may be due to the fact that the biceps brachii may have reached its load threshold when the participant lifted near-limit weights, making it impossible to recruit additional muscle fibers. The body may then attempt to use a different strategy or rely on auxiliary muscles to facilitate the lift, potentially causing a

https://doi.org/10.1021/acsmeasuresciau.3c00043
ACS Meas. Sci. Au 2024, 4, 81−91

reduction in biceps activity and further decreasing the RMS. It is worth noting that measurements taken with the MXene paper electrode were remarkably sensitive and consistent, demonstrating its superior performance in capturing shifts in muscle activity, establishing it as an exemplary choice for assessing muscle activity.

3.8. Breathability and Electrothermal Performance of the MXene Nanosheet-Based Paper Electrode

As shown in Figure 5(a), this study evaluated the breathability of various materials used as skin patch electrodes. The experiment used 20 mL glass vials containing 10 mL of ultrapure water, sealed with the material to be tested, and placed in a well-ventilated environment at 25 °C (Figure S3). Ag/AgCl electrodes were selected for comparison due to their widespread use in measuring EMG signals and to better highlight the improved breathability of our MXene paper electrodes. Under controlled conditions, we monitored variations in the weight of the water content in the vials. The control group consisted of uncovered vials, and then ordinary Xuan paper was tested. Among the groups tested, the commercial Ag/AgCl electrode showed minimal breathability, with negligible weight change observed, indicating that prolonged use may impede skin respiration, compromising comfort and potentially causing discomfort. In contrast, our MXene paper electrode exhibited superior breathability in this study with an M/M_0 ratio of approximately 0.94, suggesting that its application as a skin patch electrode could provide increased comfort and improved long-term stability. In addition, the results showed comparable breathability between MXene paper and traditional Xuan paper, meaning that the MXene coating did not significantly affect the breathability of the Xuan paper fibers.

As illustrated in Figure 5(b), the electrothermal performance of the MXene paper electrode was plotted at various voltage levels. The data distinctly indicated that as the voltage increased, the temperature of the MXene paper electrode also rose, a finding substantiated by its corresponding infrared images (Figure 5(c)). The electrothermal performance stability was confirmed by nearly superimposed temperature curves from the first to the 30th cycle during the cyclic heating/cooling of MXene paper electrode at 5 V, as shown in Figure S4. At the minimum voltage of 1 V, the temperature exhibited a slight increment from the initial 28.1 to 28.7 °C. However, with a voltage elevation to 6 V, there was a sharp temperature surge, escalating from 28 °C to an impressive 64.1 °C. This marked temperature increase was particularly prominent within the initial 10 s. Subsequently, after the 150 s mark, upon power termination, the temperature exhibited a rapid decline, returning to a value close to its initial ambient state. This electrothermal behavior underscored the commendable electrothermal conversion efficiency of the MXene paper electrode. Notably, at elevated voltage levels, its capacity for rapid heating positioned it advantageously for applications necessitating swift thermal responses. Additionally, the rapid temperature reduction post-power-off highlighted a favorable thermal dispersion attribute of the MXene paper electrode. Of significance, the MXene paper electrode could generate substantial Joule heat even within voltage thresholds considered safe for human use, showcasing its significant potential in wearable electrothermal devices. In addition, if one wants to further improve the electrothermal performance of the MXene paper electrode, one can refer to the research of Shu et al.[31] who incorporated interdigitated electrode structures into the MXene paper electrode to achieve improved electrothermal performance.

3.9. Environmentally Friendly Method for Decomposing MXene Paper Electrode

In this study, we used a 5 M NaOH solution to decompose the MXene paper electrode. As shown in Figure 5(d), after 1 h of treatment, slight decomposition of the MXene paper electrode was evident. When the treatment time was extended to 12 h, the MXene paper electrode was completely decomposed, leaving only suspended fibers. The literature has also reported that MXene is oxidized to TiO_2 in the presence of NaOH, which explains the absence of the characteristic black hue of MXene in the final decomposed images.[29] This decomposition behavior has profound implications for environmental protection and e-waste reduction. Such a characteristic of the MXene paper electrode suggests that it can rapidly decompose in the environment after its operational life cycle, thereby limiting long-term environmental pollution. Importantly, the resulting titanium dioxide after decomposition is an environmentally benign substance, further strengthening the potential of the MXene paper electrode as a green material.

4. CONCLUSIONS

The development and optimization of MXene nanosheet-based paper electrodes showcased their remarkable versatility and adaptability across a plethora of applications, particularly in green electronics. Cellulose-based materials, specifically Xuan paper, emerged as the premier choice for substrate due to their mechanical robustness, inherent flexibility, and extraordinary capacity to host MXene.[34,35] Xuan paper also exhibited superior electrical conductivity, fostering an efficient conductive network that is essential for EMG signal capture.

The optimized MXene paper electrode's consistent conductivity, even under varying bending conditions, underscores its significant potential in dynamic scenarios like wearable devices, electronic skins, and other flexible electronics. Its demonstrated utility in circuits, illuminating LEDs, and high breathability further accentuate its applicability in real-world electronics and medical devices. Furthermore, the MXene paper electrode demonstrates remarkable electrothermal performance, heating quickly within safe voltage limits, making it an ideal choice for wearable electrothermal devices. Its environmentally friendly design allows it to decompose in an eco-conscious manner, leaving behind harmless substances, highlighting its potential as a green material for the future. In summary, MXene-based paper electrodes excel in versatility across medical and technological uses while aligning with sustainable design principles. This research opens promising avenues for integrating these electrodes into futuristic applications that balance performance with environmental responsibility. Additionally, MXene paper electrodes extend their utility beyond the EMG signal measurement and electrical heating. They find potential applications as electrodes in energy storage devices like supercapacitors and batteries as well as in electromagnetic shielding and active filtration layers. Future research will delve into exploring and discussing these diverse applications further.

https://doi.org/10.1021/acsmeasuresciau.3c00043
ACS Meas. Sci. Au 2024, 4, 81−91

■ ASSOCIATED CONTENT

Supporting Information

The Supporting Information is available free of charge at https://pubs.acs.org/doi/10.1021/acsmeasuresciau.3c00043.

Contents of EMG signal collection system, connection of MXene paper electrode and wire, breathability experiment setup, and electrothermal performance stability (PDF)

Special Issue Paper

Published as part of *ACS Measurement Science Au* virtual special issue "2023 Rising Stars".

■ AUTHOR INFORMATION

Corresponding Author

Tzu-En Lin − *Institute of Biomedical Engineering, National Yang Ming Chiao Tung University, 30010 Hsinchu, Taiwan; Department of Electrical and Computer Engineering, College of Electrical and Computer Engineering, National Yang Ming Chiao Tung University, 30010 Hsinchu, Taiwan;* orcid.org/0000-0003-4291-3601; Email: telin@nycu.edu.tw

Authors

Shan-Chu Yu − *Institute of Biomedical Engineering, National Yang Ming Chiao Tung University, 30010 Hsinchu, Taiwan*

Tzu-Yen Huang − *Kaohsiung Medical University Hospital, Kaohsiung Medical University, 807378 Kaoshiung, Taiwan*

Complete contact information is available at: https://pubs.acs.org/10.1021/acsmeasuresciau.3c00043

Author Contributions

CRediT: **Shan-Chu Yu** data curation, formal analysis, investigation, methodology, validation, writing-original draft, writing-review & editing; **Tzu-Yen Huang** methodology, supervision, writing-review & editing; **Tzu-En Lin** conceptualization, project administration, supervision, writing-review & editing.

Funding

This work was supported by the Young Scholar Fellowship Program of the NSTC in Taiwan [grant numbers 112-2636-E-A49-007 and 112-2221-E-A49-051].

Notes

Ethical consent: Ethical approval for the involvement of human subjects in this study was granted by Institutional Review Board of Kaohsiung Medical University Hospital, Reference number KMUHIRB-E(I)-20230179.

Declaration of Generative AI and AI-Assisted Technologies in the Writing Process: During the preparation of this work, the authors used ChatGPT 4.0 in order to check the grammar of the texts. After using this service, the authors reviewed and edited the content as needed and took full responsibility for the content of the publication.

The authors declare no competing financial interest.

■ REFERENCES

(1) Kiddee, P.; Naidu, R.; Wong, M. H. Electronic Waste Management Approaches: An Overview. *Waste Manage.* **2013**, *33* (5), 1237−1250.

(2) Shahabuddin, M.; Uddin, M. N.; Chowdhury, J. I.; Ahmed, S. F.; Uddin, M. N.; Mofijur, M.; Uddin, M. A. A Review of the Recent Development, Challenges, and Opportunities of Electronic Waste (e-Waste). *Int. J. Environ. Sci. Technol.* **2023**, *20* (4), 4513−4520.

(3) Corzo, D.; Rosas-Villalva, D.; C, A.; Tostado-Blázquez, G.; Alexandre, E. B.; Hernandez, L. H.; Han, J.; Xu, H.; Babics, M.; De Wolf, S.; Baran, D. High-Performing Organic Electronics Using Terpene Green Solvents from Renewable Feedstocks. *Nat. Energy* **2023**, *8* (1), 62−73.

(4) Cantarella, G.; Madagalam, M.; Merino, I.; Ebner, C.; Ciocca, M.; Polo, A.; Ibba, P.; Bettotti, P.; Mukhtar, A.; Shkodra, B.; Inam, A. S.; Johnson, A. J.; Pouryazdan, A.; Paganini, M.; Tiziani, R.; Mimmo, T.; Cesco, S.; Münzenrieder, N.; Petti, L.; Cohen, N.; Lugli, P. Laser-Induced, Green and Biocompatible Paper-Based Devices for Circular Electronics. *Adv. Funct. Mater.* **2023**, *33* (17), No. 2210422.

(5) Mansoori, A.; Ahmad, S.; Bansal, S.; Vashishath, M. Flexible Graphite-Based Humidity Sensor Using Green Technology. *ECS Sens. Plus* **2022**, *1* (4), No. 044401.

(6) Su, Z.; Yang, Y.; Huang, Q.; Chen, R.; Ge, W.; Fang, Z.; Huang, F.; Wang, X. Designed Biomass Materials for "Green" Electronics: A Review of Materials, Fabrications, Devices, and Perspectives. *Prog. Mater. Sci.* **2022**, *125*, No. 100917.

(7) Irimia-Vladu, M. Green" Electronics: Biodegradable and Biocompatible Materials and Devices for Sustainable Future. *Chem. Soc. Rev.* **2014**, *43* (2), 588−610.

(8) Zhu, H.; Luo, W.; Ciesielski, P. N.; Fang, Z.; Zhu, J. Y.; Henriksson, G.; Himmel, M. E.; Hu, L. Wood-Derived Materials for Green Electronics, Biological Devices, and Energy Applications. *Chem. Rev.* **2016**, *116* (16), 9305−9374.

(9) Jin, J.; Lee, D.; Im, H.-G.; Han, Y. C.; Jeong, E. G.; Rolandi, M.; Choi, K. C.; Bae, B.-S. Chitin Nanofiber Transparent Paper for Flexible Green Electronics. *Adv. Mater.* **2016**, *28* (26), 5169−5175.

(10) Li, W.; Liu, Q.; Zhang, Y.; Li, C.; He, Z.; Choy, W. C. H.; Low, P. J.; Sonar, P.; Kyaw, A. K. K. Biodegradable Materials and Green Processing for Green Electronics. *Adv. Mater.* **2020**, *32* (33), No. 2001591.

(11) Hui, Z.; Zhang, L.; Ren, G.; Sun, G.; Yu, H.-D.; Huang, W. Green Flexible Electronics: Natural Materials, Fabrication, and Applications. *Adv. Mater.* **2023**, *35* (28), No. 2211202.

(12) Silvestre, S. L.; Pinheiro, T.; Marques, A. C.; Deuermeier, J.; Coelho, J.; Martins, R.; Pereira, L.; Fortunato, E. Cork Derived Laser-Induced Graphene for Sustainable Green Electronics. *Flex. Print. Electron.* **2022**, *7* (3), No. 035021.

(13) Fu, Q.; Chen, Y.; Sorieul, M. Wood-Based Flexible Electronics. *ACS Nano* **2020**, *14* (3), 3528−3538.

(14) Xu, J.; Zhao, X.; Zhao, X.; Wang, Z.; Tang, Q.; Xu, H.; Liu, Y. Memristors with Biomaterials for Biorealistic Neuromorphic Applications. *Small Sci.* **2022**, *2* (10), No. 2270020.

(15) Lovley, D. R.; Yao, J. Intrinsically Conductive Microbial Nanowires for 'Green' Electronics with Novel Functions. *Trends Biotechnol.* **2021**, *39* (9), 940−952.

(16) Monroe, M. M.; Villanueva, L. G.; Briand, D. Low-Temperature Processing of Screen-Printed Piezoelectric $KNbO_3$ with Integration onto Biodegradable Paper Substrates. *Microsyst. Nanoeng.* **2023**, *9* (1), 19.

(17) Min, J.; Jung, Y.; Ahn, J.; Lee, J. G.; Lee, J.; Ko, S. H. Recent Advances in Biodegradable Green Electronic Materials and Sensor Applications. *Adv. Mater.* **2023**, 2211273 DOI: 10.1002/adma.202211273.

(18) Tong, R.; Ma, Z.; Yao, R.; Gu, P.; Li, T.; Liu, L.; Guo, F.; Zeng, M.; Xu, J. Stretchable and Transparent Alginate Ionic Gel Film for Multifunctional Sensors and Devices. *Int. J. Biol. Macromol.* **2023**, *246*, No. 125667.

(19) Liu, W.; Liu, K.; Du, H.; Zheng, T.; Zhang, N.; Xu, T.; Pang, B.; Zhang, X.; Si, C.; Zhang, K. Cellulose Nanopaper: Fabrication, Functionalization, and Applications. *Nano-Micro Lett.* **2022**, *14* (1), 104.

(20) Tobjörk, D.; Österbacka, R. Paper Electronics. *Adv. Mater.* **2011**, *23* (17), 1935−1961.

(21) Lim, K. R. G.; Shekhirev, M.; Wyatt, B. C.; Anasori, B.; Gogotsi, Y.; Seh, Z. W. Fundamentals of MXene Synthesis. *Nat. Synth.* **2022**, *1* (8), 601−614.
(22) Naguib, M.; Kurtoglu, M.; Presser, V.; Lu, J.; Niu, J.; Heon, M.; Hultman, L.; Gogotsi, Y.; Barsoum, M. W. Two-Dimensional Nanocrystals Produced by Exfoliation of Ti3AlC2. *Adv. Mater.* **2011**, *23* (37), 4248−4253.
(23) VahidMohammadi, A.; Rosen, J.; Gogotsi, Y. The World of Two-Dimensional Carbides and Nitrides (MXenes). *Science* **2021**, *372* (6547), No. eabf1581.
(24) Mohammadniaei, M.; Koyappayil, A.; Sun, Y.; Min, J.; Lee, M.-H. Gold Nanoparticle/MXene for Multiple and Sensitive Detection of oncomiRs Based on Synergetic Signal Amplification. *Biosens. Bioelectron.* **2020**, *159*, No. 112208.
(25) Medetalibeyoglu, H.; Beytur, M.; Akyıldırım, O.; Atar, N.; Yola, M. L. Validated Electrochemical Immunosensor for Ultra-Sensitive Procalcitonin Detection: Carbon Electrode Modified with Gold Nanoparticles Functionalized Sulfur Doped MXene as Sensor Platform and Carboxylated Graphitic Carbon Nitride as Signal Amplification. *Sens. Actuators, B* **2020**, *319*, No. 128195.
(26) Lin, X.; Li, C.; Meng, X.; Yu, W.; Duan, N.; Wang, Z.; Wu, S. CRISPR-Cas12a-Mediated Luminescence Resonance Energy Transfer Aptasensing Platform for Deoxynivalenol Using Gold Nanoparticle-Decorated $Ti_3C_2T_x$ MXene as the Enhanced Quencher. *J. Hazard. Mater.* **2022**, *433*, No. 128750.
(27) Jeon, M.; Jun, B.-M.; Kim, S.; Jang, M.; Park, C. M.; Snyder, S. A.; Yoon, Y. A Review on MXene-Based Nanomaterials as Adsorbents in Aqueous Solution. *Chemosphere* **2020**, *261*, No. 127781.
(28) Yang, P.; Xia, T.; Ghosh, S.; Wang, J.; Rawson, S. D.; Withers, P. J.; Kinloch, I. A.; Barg, S. Realization of 3D Epoxy Resin/$Ti_3C_2T_x$ MXene Aerogel Composites for Low-Voltage Electrothermal Heating. *2D Mater.* **2021**, *8* (2), No. 025022.
(29) Doo, S.; Chae, A.; Kim, D.; Oh, T.; Ko, T. Y.; Kim, S. J.; Koh, D.-Y.; Koo, C. M. Mechanism and Kinetics of Oxidation Reaction of Aqueous Ti3C2Tx Suspensions at Different pHs and Temperatures. *ACS Appl. Mater. Interfaces* **2021**, *13* (19), 22855−22865.
(30) Cao, M.; Wang, F.; Wang, L.; Wu, W.; Lv, W.; Zhu, J. Room Temperature Oxidation of Ti_3C_2 MXene for Supercapacitor Electrodes. *J. Electrochem. Soc.* **2017**, *164* (14), A3933.
(31) Shekhirev, M.; Shuck, C. E.; Sarycheva, A.; Gogotsi, Y. Characterization of MXenes at Every Step, from Their Precursors to Single Flakes and Assembled Films. *Prog. Mater. Sci.* **2021**, *120*, No. 100757.
(32) Shuck, C. E.; Sarycheva, A.; Anayee, M.; Levitt, A.; Zhu, Y.; Uzun, S.; Balitskiy, V.; Zahorodna, V.; Gogotsi, O.; Gogotsi, Y. Scalable Synthesis of $Ti_3C_2T_x$ MXene. *Adv. Eng. Mater.* **2020**, *22* (3), No. 1901241.
(33) Satheeshkumar, E.; Makaryan, T.; Melikyan, A.; Minassian, H.; Gogotsi, Y.; Yoshimura, M. One-step Solution Processing of Ag, Au and Pd@MXene Hybrids for SERS. *Sci. Rep.* **2016**, *6*, No. 32049.
(34) Deng, L.; Zhang, Y.; Wei, S.; Lv, H.; Chen, G. Highly Foldable and Flexible Films of PEDOT:PSS/Xuan Paper Composites for Thermoelectric Applications. *J. Mater. Chem. A* **2021**, *9* (13), 8317−8324.
(35) Dong, L.-Y.; Zhu, Y.-J. Fire-Resistant Inorganic Analogous Xuan Paper with Thousands of Years' Super-Durability. *ACS Sustainable Chem. Eng.* **2018**, *6* (12), 17239−17251.

https://doi.org/10.1021/acsmeasuresciau.3c00043
ACS Meas. Sci. Au 2024, 4, 81−91